Reprinted from JOURNAL OF THE ELECTROCHEMICAL SOCIETY
Vol. 139, No. 5, May 1992
Printed in U.S.A.

Improvement to Bulk Oxygen Precipitate Density Necessary for Internal Gettering in Antimony Doped N/N$^+$ Epitaxial Wafers Using the 3-Step Technique and Ramped Nucleation

Alain R. Comeau*

Mitel Semiconductor, Bromont, Québec, Canada, J0E 1L0

ABSTRACT

The addition of a ramped nucleation cycle, just after an initial oxidation, is shown to greatly increase the precipitation of interstitial oxygen during simulated processing on N/N$^+$ antimony doped epitaxial wafers. When used with fully processed wafers, the ramped nucleation improves internal gettering. Oxygen precipitate density and bulk stacking fault density achieved are about a factor of 100 higher when using ramped nucleation. These results indicate that N/N$^+$ antimony doped epitaxial wafers have an intrinsic gettering capability as good as that of lightly doped material when using an activation cycle (initial oxidation) and subsequent ramped nucleation. A method for calculating bulk stacking fault density is presented. It is shown that, at high concentration (above 10^7 cm^{-3}), the square of the bulk stacking fault length is inversely proportional to their density. This finding indicates that the growth of bulk stacking faults is limited by the supply of interstitial silicon generated in the bulk during oxygen precipitate growth.

Gettering in highly doped antimony substrates, used for epitaxial wafers, is a major concern, especially regarding gate oxide and diode integrity. Significant efforts have been made to achieve good gettering in N/N$^+$ antimony doped epitaxial wafers (1-6). The retardation of oxygen precipitation in this material has been attributed to the difficulty of incorporating oxygen during crystal growth (7) of the highly antimony doped crystal. Some models involving electrical effects to explain the influence of doping level and doping species on oxygen precipitation have been proposed by some workers (8-11). More recently, Bains (12) has observed precipitation retardation in crystal doped with antimony, but not in crystal doped with tin, which has a similar ion size. They concluded that retardation in antimony doped silicon was not caused solely by the large size of antimony ions.

A typical method for achieving significant oxygen precipitation in silicon wafers, is to use low temperature (500-800°C) to grow oxygen nuclei (or clusters) prior to processing at higher temperatures where precipitation occurs. At low temperatures, nucleation is easier because there is less thermal energy to break up nuclei in formation. At higher temperatures, oxygen diffusion is increased and, for nuclei with sizes above a critical dimension, growth occurs faster (13). Typical nucleation cycles are done at constant temperature (650-750°C) for fairly long time (8-48 h) (5, 6).

The objective of this work was to experiment on N/N$^+$ antimony doped epitaxial wafers, using a method of nucleating and growing oxygen precipitates reported by Kishino (14) on lightly doped wafers. This method consists in a combination of two thermal processes (Fig. 1). First, a soak in nitrogen (N_2) at a temperature of 650°C is done. Then a temperature ramp-up to 900°C in N_2 at constant ramp rate is performed.

* Electrochemical Society Active Member.

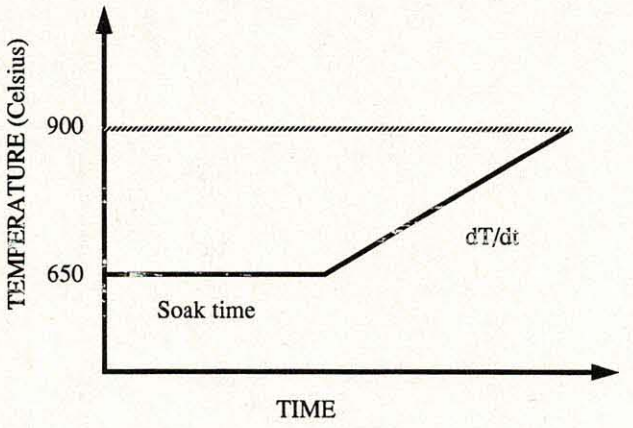

Fig. 1. Schematic representation of the thermal cycle discussed by Kishino (14), and also in this work.

Kishino experimented with different soak times and different ramp-up rates. Values similar to the ones he reported were used in this work. Ramping to 1000°C was also experimented with in this work. Ramping up to 1000°C is expected to grow larger nuclei, which are less likely to be dissolved during subsequent higher temperature cycles.

The next section describes the experimental procedure used in this experiment. Then, the experimental results are discussed. The discussions focus on the precipitation of oxygen, the methodology for measuring bulk defect density, the bulk stacking fault size dependence, the measures of wafer bow, and, finally, on the gettering capability of fully processed wafers.

Experimental

100 mm (100) n^-/n^+ epitaxial wafers were used with substrates antimony doped to 30-50 mΩ-cm. The epitaxial layer was lightly doped with phosphorus and nominally 10 μm thick. The oxygen content of each wafer was measured before any processing was done. All wafers were within 15.7-16.3 atomic part per million (ppmA) range (ASTM-F121-83). Carbon content was specified to be less than 1.0 ppmA. The substrate used for these wafers is somewhat less heavily doped than the usual antimony doped epitaxial substrate (8-15 mΩ-cm), this enables the oxygen content to be measured by conventional infrared techniques. Because of the lower doping level, some oxygen precipitation has been found to occur in similar substrates (5) when long nucleation times are used.

For process simulation (Fig. 2), the most important front end thermal cycles were used in sequence (Initial oxidation, Nucleation-Growth, Well diffusion, and Field oxidation). The main difference between actual process front end and process simulation is the absence of subnitride oxidation and nitride deposition before field oxidation. Studies of the evolution of oxygen precipitation have revealed that this difference is not significant (15) for oxygen precipitation, even though nitride deposition is done at temperatures close to 800°C, where interstitial oxygen may precipitate.

Nucleation-growth (NG) was inserted after initial oxide (1175°C/35 min) and before well diffusion (1175°C/400 min). In Kishino (14), a NG cycle was inserted after a cycle of 3 h at 1200°C and before a cycle of 16 h at 1000°C. These differences in processing temperatures and times may lead to differences in oxygen precipitation. For example, it has been found (15) that oxygen nucleation is retarded if long times are spent at high temperatures before NG is done.

The NG cycles with which we experimented are described in Table I. The soak was always done at 650°C for periods of 1, 2, and 4 h. Ramping from 650 up to 900 or 1000°C was experimented with at 1, 2, and 4 deg/min. Total cycle times were between 122.5 and 590 min. Two wafers were used per split. Twelve wafers were also processed without any NG cycle to serve as references. Two of these wafers had very high oxygen content, about 21 ppmA.

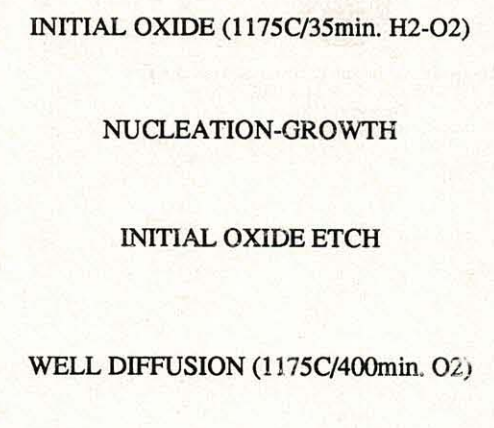

Fig. 2. Simulated process used for the wafers in this experiment.

Once the simulated process was completed, wafer bow was measured using interferometry and the final interstitial oxygen content was measured by infrared spectrophotometry (ASTM-F121-83). Then the wafers were cleaved and had a Wright etch (16) for 1 min to delineate surface and bulk defects. Phase contrast pictures of wafer sections were taken near the wafer center to count bulk defects (precipitates, and stacking faults). Some pictures were also taken near the wafer edges for comparison.

Most often, gettering ability can be evaluated by any of four methods; two indirect, one relative, and one absolute. In this work, the two indirect methods and the relative method were used. The two indirect methods consist of measuring the amount of precipitated oxygen after simulated processing (ΔO_i), and counting the number of bulk defects after preferential etching of a section. The relative method consists of processing a number of wafers with standard processing and wafers with experimental processing. Results from each split are then compared for gate oxide and/or diode integrity.

The absolute method consists of intentionally contaminating a sample and measuring the amount of electrically active contamination after processing (17). This method was not used in this experiment.

Table I. Total time in minutes for each experimental combinations of soak time and ramping rate.

	Total NG cycle time		
RAMP to 900°C Soak at 650°C:	1.0 h	2.0 h	4.0 h
4.0 deg/min	122.5	182.5	302.5
2.0 deg/min	185.0	245.0	365.0
1.0 deg/min	310.0	370.0	490.0
RAMP to 1000°C Soak at 650°C:	1.0 h	2.0 h	4.0 h
4.0 deg/min	147.5	207.5	327.5
2.0 deg/min	235.0	295.0	415.0
1.0 deg/min	410.0	470.0	590.0

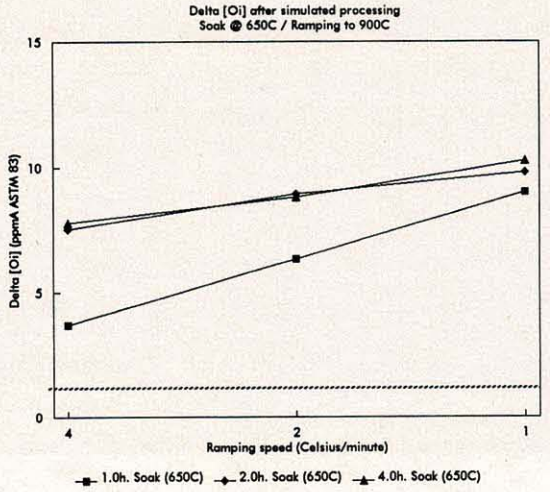

Fig. 3. Precipitated oxygen in wafers with nucleation-growth cycle (NG) ramp to 900°C. The quantity of precipitated oxygen is about a factor of 10 higher than without NG (dash line). Little difference is seen between 2.0 and 4.0 h soak.

Results and Discussion

Oxygen precipitation.—Oxygen precipitation (ΔO_i) results are presented in Fig. 3 (ramping to 900°C) and Fig. 4 (ramping to 1000°C). As a reference, a change of 1 ppmA in interstitial oxygen concentration was observed on wafers without NG (with identical initial oxygen content). Part of the interstitial oxygen loss is due to oxygen out diffusion (0.5 ppmA calculated). Ramping to 900 or 1000°C made little difference except when the ramping rate was 2°C/min, in which case ramping to 1000°C yielded significantly higher oxygen precipitation for all three soak times.

It is interesting to note the importance of the oxygen precipitation in these epitaxial wafers. Each wafer used for NG had an initial oxygen content between 15.7-16.3 ppmA (16.0 ppmA will be assumed in the following discussion). The least amount of precipitation (ΔO_i = 3.5 ppmA) observed with NG (1 h/650°C and 4°C/min ramp up to 950°C) is about six times higher than the simulated process with no NG cycle (excluding oxygen outgasing).

Wafers with O_i = 21 ppmA which did not have NG showed ΔO_i = 4 ppmA, which is comparable to the least amount of precipitation observed with NG. The most important precipitation observed with NG (ΔO_i = 10.8 ppmA) was obtained on wafers having a 4 h soak and ramping at 1°C/min up to 1000°C. Such a level of precipitation leaves a mere 5.2 ppmA of interstitial oxygen in the wafer.

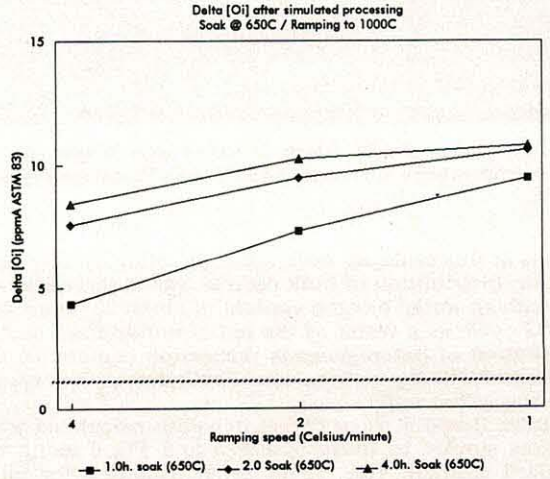

Fig. 4. Precipitated oxygen in wafers with nucleation-growth cycle (NG) ramp to 1000°C. The quantity of precipitated oxygen is comparable to the case of 900°C. Again here, the 2.0 and 4.0 h soak are not much different.

According to Craven (18) the solubility limit of oxygen at 1000°C (Field oxidation) is about 2.6 ppmA, and at 1175°C (Well drive) is 8.2 ppmA. An interstitial oxygen residual level of 5.2 ppmA indicates that some level of precipitation must occur during field oxidation for our process (5.2 ppmA is less than the 8.2 ppmA predicted by the solubility limit at 1175°C). If this is the case, then precipitate growth must occur during P-well diffusion. The maximum ΔO_i possible after well diffusion (400 min at 1175°C) is 7.8 ppmA (solubility limit is 8.2 ppmA). Preliminary step by step studies of precipitation confirm this hypothesis (15).

Precipitate growth during well diffusion probably slows down near ΔO_i = 7-8 ppmA, because the interstitial oxygen concentration is very close to the solubility limit and because precipitation kinetics are strongly dependent on supersaturated O_i concentration (19). This can explain the saturation effect observed in Fig. 4 for slower ramp rates. It also explains why curves for different soak times seem to converge to about 11 ppmA (maximum ΔO_i after field oxidation). Once all the curves are merged together, the increase could continue asymptotically to ΔO_i maximum, about 13.4 ppmA (16.0-2.6 ppmA), if more time was spent at 1000°C.

In the simulated process sequence used here, there is no significant time spent at temperatures below 900°C without NG cycle. It is well documented that such low temperatures (600-800°C) cause oxygen nucleation. This indicates that precipitation is controlled by a low temperature mechanism (nucleation) in the conditions used here. Furuya (13) has shown that heterogeneous nucleation can also be enhanced by a high temperature (1280°C) before nucleation, presumably by point defect clusters. In the case studied here, such a mechanism is also conceivable because a high temperature (1175°C) cycle precedes nucleation. More work is needed to confirm this hypothesis; in particular, the effect of temperature and time spent at high temperature have to be determined.

In order to estimate the most efficient use of furnace time *vs.* oxygen precipitation, calculations of the ratio of oxygen precipitation to the square root of extra furnace time (Table II) were conducted. The square root of time is arbitrarily used because extra time is less important, in this case, than the end result, precipitation of oxygen. According to Table II, the cycle which provides the optimum ratio of oxygen precipitation to the square root of extra furnace time is 2 h at 650°C and 2.0°C/min ramp-up to 900°C.

Defect density using the standard method.—The standard method used to estimate the bulk defect density assumes that exactly 1.0 μm of silicon was etched, the sample picture area (3×10^{-3} cm^2) is representative of the wafer, and that defects are smaller than 1 μm. The exact thickness of silicon removed is only of relative importance because all the wafers are etched at the same time and are expected to have seen the same etch rate. On the other hand, the assumption that the measured area is representative of the wafer, is not rigorous. It was only to avoid the

Table II. Ratio of extra precipitated interstitial oxygen to the square root of extra processing time. Units are ppmA/min$^{1/2}$. The square root of time is used because time is less important than precipitated oxygen level.

Optimum NG cycle analysis			
RAMP to 900°C Soak at 650°C:	1.0 h	2.0 h	4.0 h
4.0 deg/min	23	37	44
2.0 deg/min	46	49	45
1.0 deg/min	38	40	41
RAMP to 1000°C Soak at 650°C:	1.0 h	2.0 h	4.0 h
4.0 deg/min	25	39	40
2.0 deg/min	42	47	43
1.0 deg/min	39	44	39

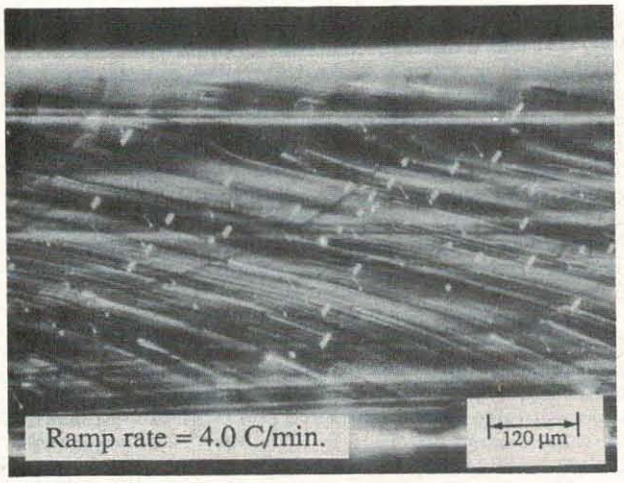

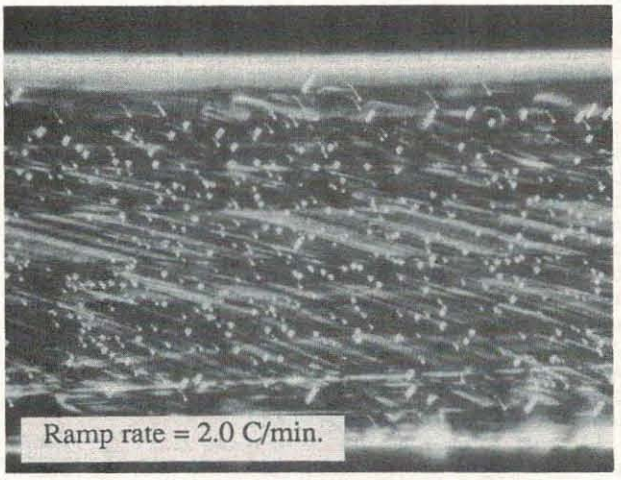

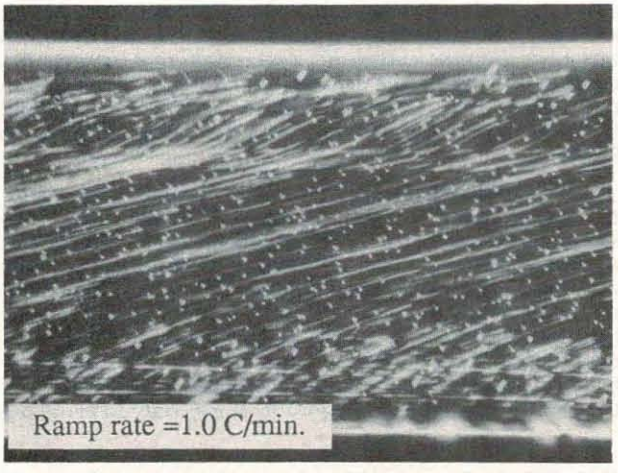

Fig. 5. Pictures of bulk defects in wafers after Wright etch for 1.0 min. Wafers had a 2.0 h soak at 650°C and different ramp rates to 900°C.

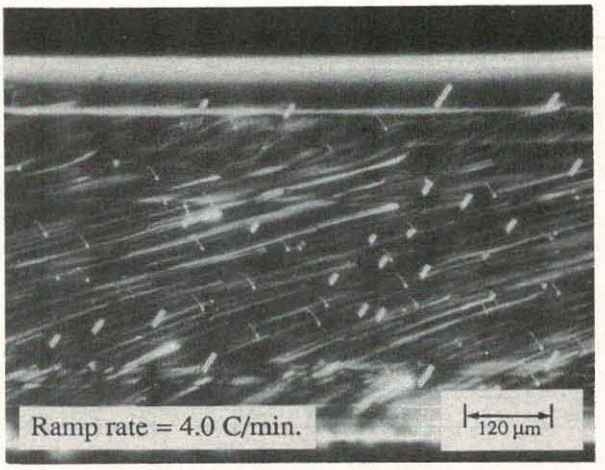

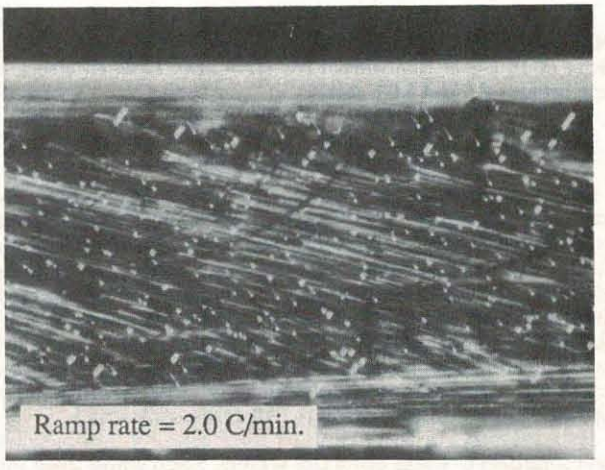

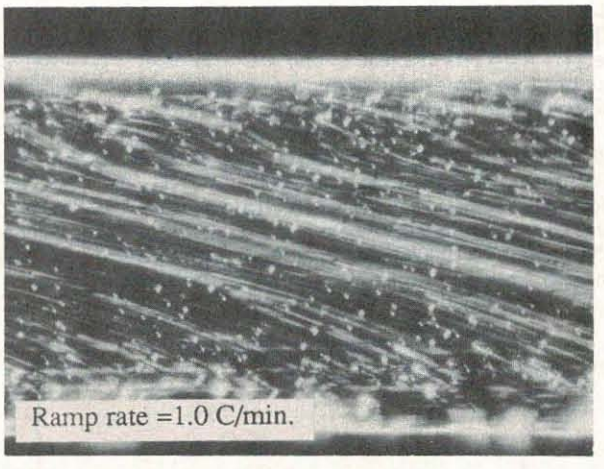

Fig. 6. Pictures of bulk defects in wafers after Wright etch for 1.0 min. Wafers had a 2.0 h soak at 650°C and different ramp rates to 1000°C.

effect of systematic spatial distribution that pictures were always taken near wafer center. The last assumption, that defects are smaller than 1.0 μm, is valid for oxygen precipitates (20-22), which have been shown to be typically less than 2000 Å, but not for bulk stacking faults (BSF). The standard defect density calculation does not take into account the size of BSF. This will be shown later to lead to significant differences in results interpretation.

To understand a little more about bulk defects, pictures of wafer sections following a 1 min Wright etch were taken. Figure 5 and 6 present such sets of typical pictures for wafers having a 2 h soak at 650°C with different ramp rate to 900°C (Fig. 5) or to 1000°C (Fig. 6). Most of the visible defects at this scale are bulk stacking faults. A very nonuniform distribution of bulk defects was observed in wafers with an initial oxygen content of about 20 ppmA and no NG cycle as a result of the initial nonuniform spatial distribution of heterogeneous nucleation centers. In the wafers with NG the distribution of bulk defects is very uniform across the wafer.

Figures 7 and 8 show defect densities calculated from pictures similar to those in Fig. 5 and Fig. 6 using the standard method. The curves seem to flatten for ramp rates of 1 deg/min. This result is in general agreement with Kishino (14). However, split to split variation in defect density are less important than in Kishino. Also, a rather unexpected effect is that higher defect densities are observed

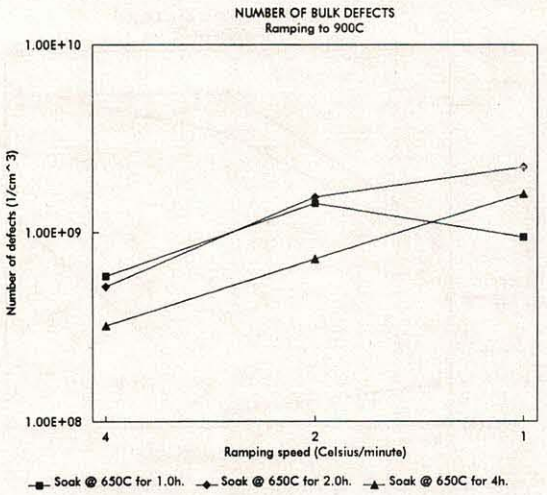

Fig. 7. Number of bulk stacking faults per unit volume for the different combinations of nucleation growth cycles with ramp to 900°C. Calculated with the usual method.

for wafers which have seen a 1 h soak at 650°C. This is an artifact of the use of the standard method to estimate defect density. To get a more accurate estimate of the defect density, the size of bulk defects must be considered. The next section deals with this issue.

Bulk stacking faults density.—An interesting feature of Fig. 5 and Fig. 6 is the range of different numbers and sizes of the defects seen. Pictures taken at higher magnification revealed more details about the bulk defects. In wafers which had slower ramp rates (Fig. 9), the most visible defects are small BSF and their number is very large. In addition to small BSF (5-7 μm), larger BSF (15-25 μm) can be observed (see Fig. 5) near the beginning of the denuded zone. When NG with faster ramp rate to 900°C (Fig. 10) is used, numerous small defects (likely to be oxygen precipitates) and some stacking faults of larger size (15-20 μm), are observed. Again here, even larger BSF are located near the beginning of the denuded zone (see Fig. 6).

Finite defect size is a feature which was neglected in the previous defect density calculation. When defect densities were computed, it was assumed that defects were much smaller than the thickness of silicon etched (1 μm). If this is not the case, then the number of defects is over estimated. As shown in Fig. 11, defects which have their centers out of the etched silicon layer, but extend in this layer, will appear after the etch. In many pictures, defects much larger than 1 μm are observed. In particular, this is the case for most bulk stacking faults.

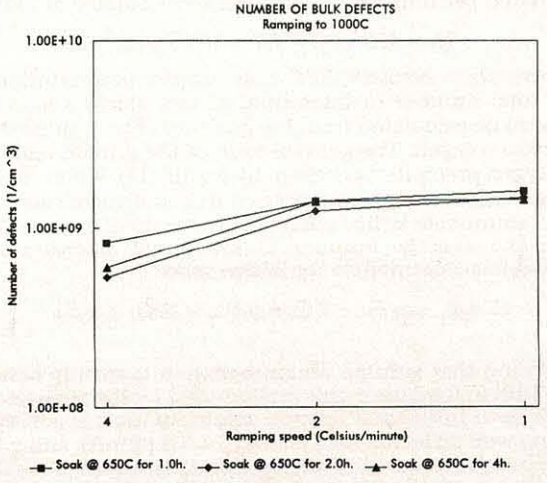

Fig. 8. Number of bulk stacking faults per unit volume for the different combinations of nucleation growth cycles with ramping to 1000°C. Calculated with the usual method.

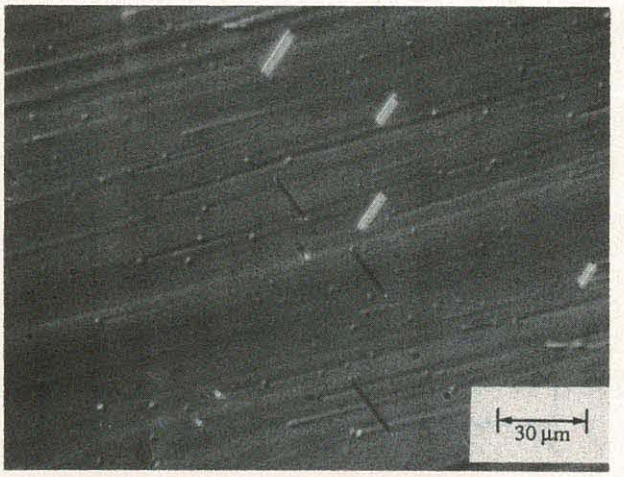

Fig. 9. Picture of bulk defects for a wafer which had 4.0 h soak at 650°C and 4.0°C/min ramp rate to 900°C.

This detrimental artifact can be compensated by assuming that all BSF in the observed area have the same real length (w), all BSF observed are circular in {111} planes (23), the thickness of silicon etched (l) is exactly 1 μm, and the observed average BSF length is $\overline{w} = \pi w/4$. Under these assumptions, the volume that is considered for defect density calculation (V) is given by Eq. [1] and is strongly dependent on defect size. This volume considers defects of length w located within the interval $[-w, 1 + w]$ from the original surface (S) to be visible in all cases

$$V = S\,(1 + 4\,\overline{w}/\pi) \quad [1]$$

$$D = n/V \quad [2]$$

Equation [2] permits accurate calculation of the defect density (D) knowing the number of defect (n) of average size $\overline{w}$. In our case, it was observed that the Wright etch failed to identify clearly BSF which intersected the cleavage plane (110) parallel to the 100 surface. This is rather unusual, and is still unexplained. To correct for this artifact, and because only two of the four possible BSF orientations were observed, the number of BSF observed (n) was multiplied by 2.

Figures 12 and 13 show the corrected BSF density for wafers which had 1, 2, or 4 h soak at 650°C. The defect densities in these figures is at least half an order of magnitude less than those calculated using the standard method (Fig. 7 and Fig. 8). Also, variations from split to split seem more consistent with oxygen precipitation data. In particular, wafers with shorter soak time at 650°C exhibit fewer BSF (as opposed to what is suggested by Fig. 7 and Fig. 8). From Fig. 12 and Fig. 13 it appears that a soak of at least

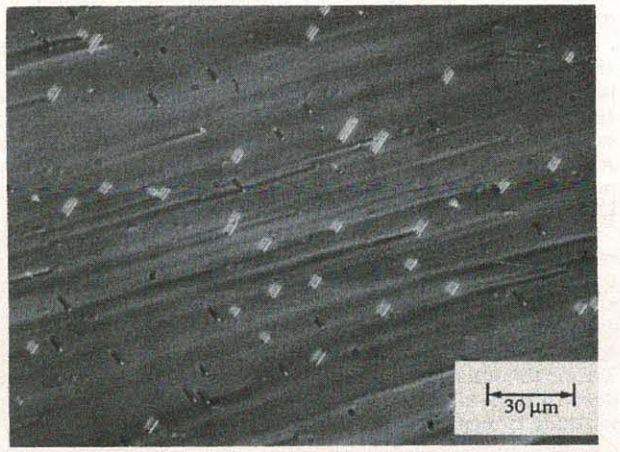

Fig. 10. Picture of bulk defects for a wafer which had 4.0 h soak at 650°C and 1.0°C/min ramp rate to 900°C.

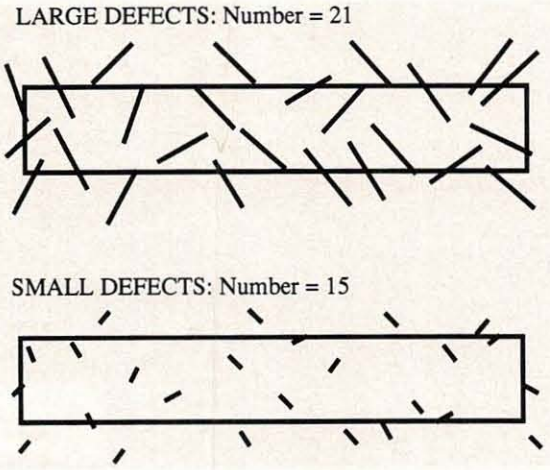

Fig. 11. Illustration of the finite size effect when counting defects from an etched section (rectangle). The number of defects (lines) which cut the lower horizontal line (original surface) or which are in the rectangle (etched volume) are counted. These defects would appear after a preferential etch. The smaller defects show smaller count despite the fact that the same density is present.

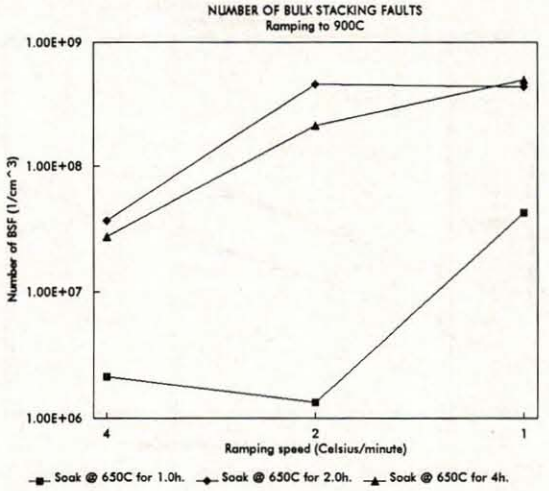

Fig. 12. Number of bulk stacking faults per unit volume corrected for bulk stacking fault size for the different combinations of nucleation growth cycles with ramping to 900°C.

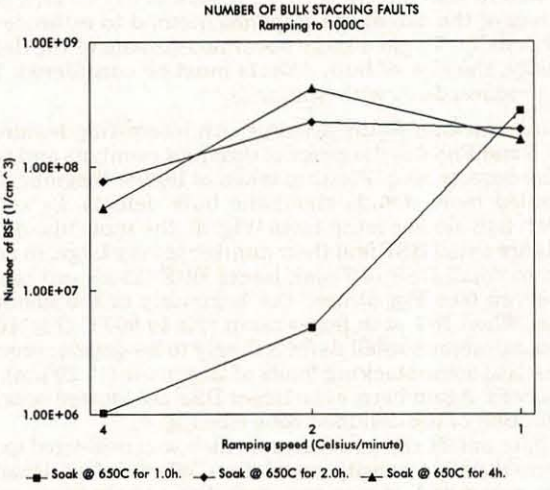

Fig. 13. Number of bulk stacking faults per unit volume corrected for bulk stacking fault size for the different combinations of nucleation growth cycles with ramping to 1000°C.

2 h is required to consistently have large BSF density. This is in agreement with results from oxygen precipitation (Fig. 3 and 4). From the observations made above, it is clear that neglecting defect size when evaluating defect density leads to erroneous conclusions.

BSF size dependence.—One possible explanation for the observed BSF size correlation with BSF density is that BSF growth reaction is limited by the supply of reactants (interstitial silicon). In this case BSF volume is inversely proportional to defect density. This would explain why BSF seen on wafers having a slower ramp rate (higher BSF density) are smaller. The fact that larger BSF are observed near the beginning of the denuded zone is different, and can be explained by the larger supply of interstitial silicon from surface oxidation (24) during well diffusion and field oxidation.

When the conditions are defects are two dimensional (like extrinsic BSF), the supply of reactant (Si_I) is the growth limiting factor, and defect size is narrowly distributed, the relationship between average defect size and defect density (D) is governed by a quadratic power law

$$D = K\sqrt{w^2} \qquad [3]$$

where K is a proportionality constant given by

$$K = \pi N_I C_I/4 \qquad [4]$$

where N_I is the number of Si_I generated per unit volume; C_I is the increase in BSF surface caused by the addition of one Si_I in the extra 111 plane. The factor $\pi/4$ is of geometrical nature.

The relation between defect size and defect density stated by Eq. [3] is strong. Figure 14 shows the observed relationship between BSF density and size for the same wafers as in Fig. 12 and 13. The BSF density was calculated with the corrected method, taking into account BSF size. Although some spread in the data points is observed, a negative square law dependence at high defect density fits the data very well, as is expected from Eq. [3].

Figure 14 also shows the expected defect size saturation at low defect density. This indicates that in wafers with actual BSF density below 10^7 cm^{-3}, the supply of interstitial silicon is not the factor limiting BSF growth, but in this case Si_I capture is the limiting factor (24). Wafers processed without NG show a BSF length of about 40 μm. This is the maximum length which can be achieved for the growth time allowed. For wafers without NG, the density is small, typically about 10^5-10^6 cm^{-3}.

Assuming that, a BSF is composed of an extra 111 plane (extrinsic stacking fault), the increase in BSF area caused by the addition of an interstitial silicon atom (C_I) is the inverse of the number of atoms per unit area in a 111 plane, *e.g.*, 5.21×10^{-16} cm^2/atom, BSF growth occurs during the well drive (see Fig. 15). Using the slope of Fig. 14 at densities above 10^7 cm^{-3} ($K = 112$ cm^{-1}), the total number of Si_I generated per unit volume (N_I) can be calculated at 1175°C

$$N_I = 4K/(\pi C_I) = 2.7 \times 10^{17}\ Si_I/cm^3 \qquad [5]$$

Correlation between BSF and oxygen precipitation.—The total number of interstitial silicon atoms generated can also be calculated from the quantity of precipitated interstitial oxygen. The general form of the growth reaction of oxygen precipitates is given by Eq. [6] (17). Where Si_v are silicon vacancies; y_1 the average number of vacancies used to accommodate lattice space; O_i is interstitial oxygen; and y_2 is the average number of interstitial silicon atoms ejected to accommodate for lattice space

$$(1 + y_1 + y_2)Si + 2\ O_i + y_1 Si_v \leftrightarrow SiO_2 + y_2 Si_I \qquad [6]$$

Assuming that volume accommodation is mainly associated with Si_I emission (this is supported by the presence of BSF), then interstitial oxygen solubility limit is achieved during well diffusion ($\Delta O_i = \Delta O_{imax} = 7.8$ ppmA), and volumetric requirement for SiO_2 (quartz) is 2.25 that of crystalline silicon, for one Si atom. Then the total number of Si_I generated by oxygen precipitation ($\overline{N}_I$) is given by

$$\overline{N}_I = \Delta O_i(2.25\text{-}1)/2 = 2.4 \times 10^{17}\ Si_I/cm^3 \qquad [7]$$

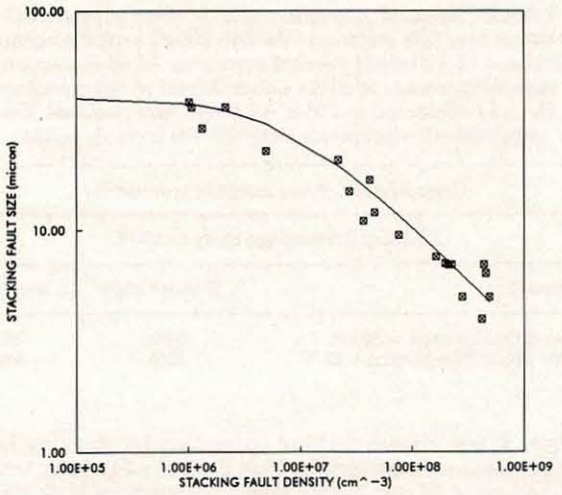

Fig. 14. Correlation between stacking fault size and density. Density was corrected for the defect size using the method described in the text. The full line is for reference only (slope is $-1/2$ above 10^7 cm^{-3}). The dash line shows the upper limit in bulk stacking fault size.

The value obtained with Eq. [7] is in excellent agreement with the experimental value calculated from the dependence of BSF length on density [5].

The agreement between the results of Eq. [5] and Eq. [7] suggests that the mechanisms assumed to describe precipitation of oxygen in our experiment are valid. Combining Eq. [5] and Eq. [7], a relation between BSF size and BSF density, which is only dependent on precipitated oxygen, is obtained

$$D = 1.25\ \pi\ C_i \Delta O_i / 8\overline{w}^2 \qquad [8]$$

This expression enables the BSF density (D) to be calculated knowing the amount of oxygen precipitated, and BSF size. Of course, D is determined by the number of nuclei whose size, obtained during nucleation, is above the minimum size for growth at precipitation temperature.

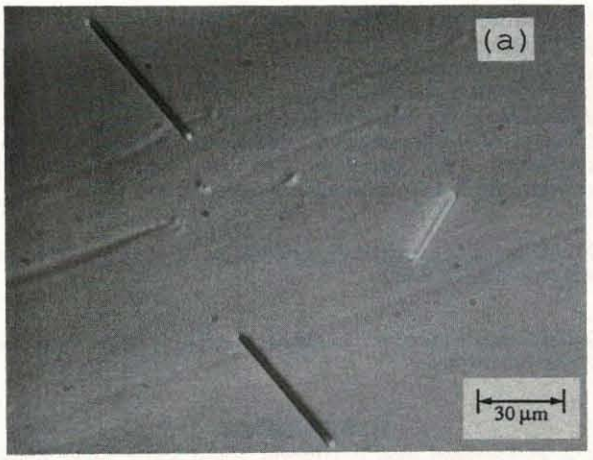

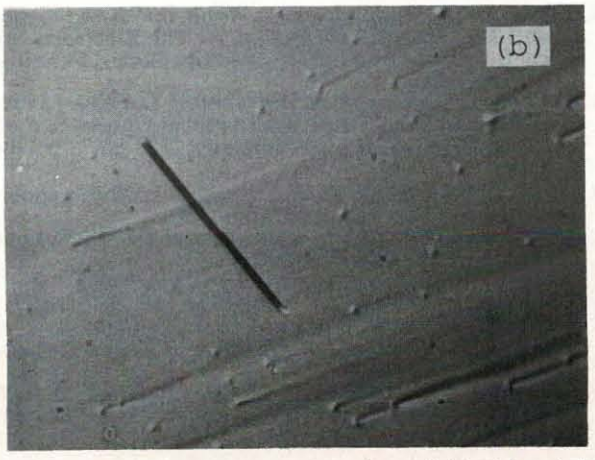

Fig. 15. Pictures showing bulk defects after well drive (a), and after field oxidation (b). Bulk stacking faults are observed to grow during well diffusion, while most isolated oxygen precipitates grow during field oxidation.

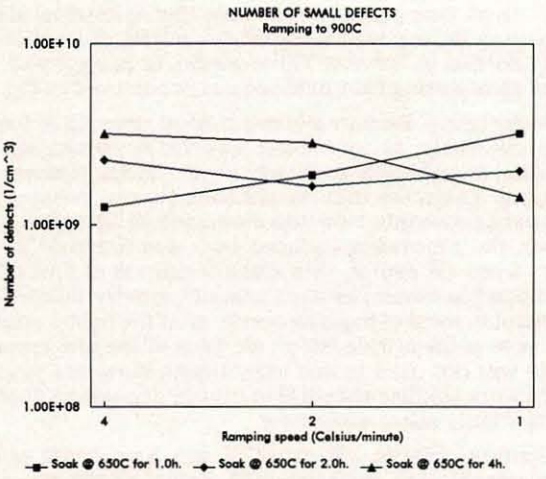

Fig. 16. Number of small defects per unit volume for the different combinations of nucleation growth cycles with ramping to 900°C.

Oxygen precipitates.—Figures 16 and 17 show the volumetric density of the small defects which are seen on high magnification pictures. The same wafers as for Fig. 12 and Fig. 13 were used. The density of small defects is about 10 times higher than the BSF density, and it varies less between splits. It also appears that the small defects density is somewhat proportional to soak time.

Ramping up to 900 or 1000°C does not make much difference in the density of small defects either, except when the soak is only 1 h. In this case, the density of small defects increases with slower ramping rates, in agreement with oxygen precipitation data. This tendency is opposite to what is observed for BSF density. From this observation, it is possible to believe that the small defects are oxygen precipitates that did not nucleate a BSF during well diffusion.

From the observation that most of the small defects (oxygen precipitates) grow during field oxidation (Fig. 15), it is interesting to ask how did oxygen nuclei survive the well drive (1175°C) since interstitial oxygen is strongly depleted (compared to the case where no BSF grow) after the

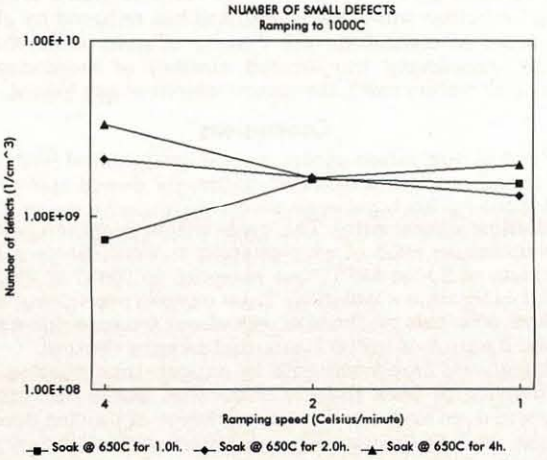

Fig. 17. Number of small defects per unit volume for the different combinations of nucleation growth cycles with ramping to 1000°C.

well drive. One possible answer is that interstitial silicon depletion during well drive allows nuclei of smaller size than normal to survive. These nuclei, or precipitates, can then grow during field oxidation as is observed in Fig. 15.

Wafer bow.—Because the mechanical strength of the wafers decreases as interstitial oxygen concentration decreases, it is possible that wafers warp during thermal processing. To ensure that the enhance oxygen precipitation does not cause this, bow was measured on all wafers. In all cases, the processing induced bow was found to be less than 2 μm. Of course, this measurement is of limited use because the normal process was not exactly followed. In particular, most of the bow occurs after the field oxidation, because of the nitride left on the back of the wafer, and nitride was not used in this experiment. However, preliminary work (15) has shown that nitride deposition does not significantly affect wafer bow.

Gettering ability.—Because Si_I is a by-product of oxygen precipitation, depletion of Si_I from the bulk, caused by the high density of BSF, favors oxygen precipitation. This means that BSF density and size control the oxygen precipitation rate along with supersaturated interstitial oxygen concentration.

The interaction between dislocations and oxygen precipitation has been noted before. In particular, high pressure crystalline SiO_2 polymorphs (coesite) has been observed in the form of small ribbons (25) along <110> dislocations. Bialas (26) has also observed that crystalline phases of SiO_2 are favored by the presence of dislocations, probably because of the high hydrostatic pressure around dislocations. The presence of high density of BSF, in the results presented here, explains why high levels of oxygen precipitation are observed in highly antimony doped substrate.

When BSF density (D) is high enough to affect BSF size, the mean free path of silicon interstitial is strongly reduced. Since fast metallic contaminants diffuse similarly to silicon interstitials, they should also be captured by BSF during cool down and see their mean free path reduced. Therefore good gettering is expected when the BSF length is affected by the BSF density.

To confirm the improved gettering of epitaxial wafers using NG, 21 wafers were processed; 9 with NG and 12 without. On each finished wafer, capacitors (8 sites) and diode integrity (5 sites) were checked.

Capacitors (250,000 μm^2) were measured for leakage at 10 V in accumulation (n- and p-substrates). A capacitor was considered short if a current greater than 30 nA was measured. The breakdown voltage of n^+/p^- diodes (185,000 μm^2) was measured at 1.0 μA. For the diodes the fail criteria was a breakdown voltage below or equal to 21 V. The process used here usually gives n^+/p^- diode breakdown voltage of 23 V.

Table III presents the results obtained. The improvement in gettering is measurable. The use of NG has probably eliminated the occurrence of contamination induced n^+/p^- junction soft-breakdown, and has reduced by about an order of magnitude the density of gate oxide shorts. Even considering the limited number of measurement sites and wafers used, the improvement is significant.

Table III. Results of gate oxide and n^+/p^- diode integrity tests. 9 wafers were fully processed with the optimum nucleation-growth (NG) and 12 wafers had standard processing. All other processing steps were common to all the wafers. A total of 168 capacitors (n- and p-substrates) and 95 n^+/p^- diodes were measured. The improvement in parametric yield with NG is clearly visible.

Capacitor and diode integrity test results		
2.0 h and 2.0 deg/min ramp to 900°C		
Parameter	Without NG	With NG
Gate oxide leakage > 30 nA	22%	3%
n^+/p^- diode breakdown < 21 V	23%	0%

Conclusions

Several nucleation cycles were experimented with after an initial oxidation on N/N^+ antimony doped substrates. All these cycles have been shown to improve oxygen precipitation significantly. The cycle which seems to provide the optimum ratio of precipitation to extra furnace time consists of 2 h at 650°C and ramp-up to 900°C at 2°C/min (total extra time = 245 min). Total oxygen precipitation obtained with this nucleation was about 9 ppmA for wafers with 16 ppmA of initial interstitial oxygen content.

Significant improvements in oxygen precipitation and in density of bulk defects show that nucleation-growth process does improve the effectiveness of oxygen precipitation. This in turn greatly improves internal gettering in wafers.

A method has been developed to calculate stacking fault volumic density, taking into account stacking faults length. It was shown that not correcting for stacking fault length when calculating stacking fault density leads to significant error. It was shown that the density of bulk stacking faults generated during simulated process was so high using a nucleation cycle that stacking fault length was limited by the supply of interstitial silicon generated in the bulk. Dependence of BSF density on BSF size showed a negative square law as expected from interstitial generation during precipitation to accommodate for precipitate volume expansion.

Finally, fully processed wafers with and without ramp nucleation were tested for gate oxide and n^+/p^- junction integrity. For both electrical measurements, a very significant improvement could be observed, confirming the efficiency of the internal gettering achieved with ramp nucleation.

Acknowledgments

The author would like to thank R/D operators for processing the experimental wafers, Cheryl Wilson for preparing all the nucleation-growth cycles, Jean Ouellet for his help with interstitial oxygen content measurements, and Linda Plouffe for measuring numerous batches of wafers, so wafers of similar oxygen content could be used in this experiment. Also, thanks go to P. Huet, for numerous discussions and his continuous encouragement.

Manuscript submitted April 9, 1991; revised manuscript received Jan. 27, 1992.

Mitel Semiconductor assisted in meeting the publication costs of this article.

REFERENCES

1. J. O. Borland and T. Deacon, *Solid State Technology*, August, 123 (1984).
2. S. Hahn, J. O. Borland, and D. Wong, in "VLSI Science and Technology," PV 85-5, p. 96, The Electrochemical Society Softbound Proceedings Series, Pennington, NJ (1985).
3. F. Secco d'Aragona, J. W. Rose, and P. L. Fejes, in Proceedings of the Third International Conference on VLSI Science and Technology, PV 85-5, p. 106 (1985).
4. J. W. Medernach, V. A. Wells, and L. L. Witherspoon, *Semicond. Int.*, February, 106 (1987).
5. W. Wijaranakula, J. H. Matlock, and H. Mollenkopf, *This Journal*, **129,** 3113 (1988).
6. J. O. Borland, *Semicond. Int.*, April, 144 (1989).
7. T. Nozaki, and Y. Itoh, *J. Appl. Phys.*, **59,** 2562 (1986).
8. D. A. P. Bulla, W. E. Castro, Jr., V. Stojanoff, F. A. Ponce, S. Hahn, and W. A. Tiller, *J. Cryst. Growth*, **85,** 91 (1987).
9. S. Hahn, F. A. Ponce, W. A. Tiller, V. Stojanoff, D. A. P. Bulla, and W. E. Castro, *J. Appl. Phys.*, **64,** 4454 (1988).
10. K. Wada, *Phys. Rev. B*, **30,** 5884 (1984).
11. K. Wada and N. Innoue, in "Semiconductor Silicon 1986," H. R. Huff, T. Abe, and B. Kolbeson, Editors, PV 86-4, p. 778, The Electrochemical Society Softbound Proceedings Series, Pennington, NJ (1986).

12. S. K. Bains, D. P. Griffiths, J. G. Wilkes, R. W. Series, and K. G. Barraclough, *This Journal*, **137,** 647 (1990).
13. H. Furuya, I. Suzuki, Y. Shimanuki, and K. Murai, *ibid.*, **135,** 677 (1988).
14. S. Kishino, T. Aoshima, A. Yoshinaka, H. Shimizu, and M. Ono, *Jpn. J. Appl. Phys.*, **23,** L9 (1984).
15. A. R. Comeau, J. J. Farber, and K. Kwong, To be published.
16. M. Wright Jenkins, *This Journal*, **124,** 757 (1977).
17. T. Y. Tan and C. Y. Kung, *J. Appl. Phys.*, **59,** 917 (1986).
18. R. A. Craven, in "Semiconductor Silicon 1981," H. R. Huff, R. J. Kriegler, and Y. Takeishi, Editors, PV 81-5, p. 344, The Electrochemical Society Softbound Proceedings Series, Princeton, NJ (1981).
19. J. Burke, in "The Kinetics of Phase Transformations in Metals," Ch. 5, Pergamon, London (1965).
20. D. Gilles, E. R. Weber, S. Hahn, and K. Cho, in "Proceedings of the International Conference on the Science and Technology of Defect Control in Semiconductors," K. Shimuno, Editor, Yokohama, Japan, Sept. 17-22 (1989).
21. F. Shimura and H. Tsuya, *This Journal*, **129,** 1062 (1982).
22. L. Rivaud, C. N. Anagnostopoulos, and G. R. Erikson, *ibid.*, **135,** 437 (1988).
23. C. L. Claeys, G. J. Declerk, and R. J. van Overstraeten, Abstract 487, p. 1237, The Electrochemical Society Extended Abstracts, Los Angeles, CA, Oct. 14-19, 1979.
24. A. Lin, R. W. Dutton, D. A. Antoniades, and W. A. Tiller, *This Journal*, **128,** 1121 (1981).
25. A. Bourret, J. Thibaut-Desseaux, and N. D. Seidman, *J. Appl. Phys.*, **55,** 825 (1986).
26. D. Bialas and J. Hesse, *J. Mater. Sci.*, **4,** 779 (1969).